Strain softening, yielding, and shear thinning in glassy colloidal suspensions

Vladimir Kobelev and Kenneth S. Schweizer*
Department of Materials Science and Engineering and Frederick Seitz Materials Research Laboratory, University of Illinois, 1304 West Green Street, Urbana, Illinois 61801, USA
(Received 24 May 2004; revised manuscript received 8 November 2004; published 2 February 2005)

A microscopic theory for the dependence on external strain, stress, and shear rate of the transient localization length, elastic modulus, alpha relaxation time, shear viscosity, and other dynamic properties of glassy colloidal suspensions is formulated and numerically applied. The approach is built on entropic barrier hopping as the elementary physical process. The concept of an ideal glass transition plays no role, and dynamical slowing down is a continuous, albeit precipitous, process with increasing colloid volume fraction. The relative roles of mechanically driven motion versus thermally activated barrier hopping and transport have been studied. Various scaling behaviors are found for the relaxation time and shear viscosity in both the controlled stress and shear rate mode of rheological experiments. Apparent power law and/or exponential dependences of the elastic modulus and perturbative and absolute yield stresses on colloid volume fraction are predicted. A nonmonotonic dependence of the absolute yield strain on volume fraction is also found. Qualitative and quantitative comparisons of calculations with experiments on high volume fraction glassy colloidal suspensions show encouraging agreement, and multiple testable predictions are made. The theory is generalizable to treat nonlinear rheological phenomena in other soft glassy complex fluids including depletion gels.

DOI: 10.1103/PhysRevE.71.021401 PACS number(s): 82.70.Dd, 61.43.Fs, 83.60.Df, 83.10.−y

I. INTRODUCTION

The dynamics of complex fluids such as concentrated colloidal suspensions, foams, slurries, pastes, emulsions, and even granular assemblies exhibit many features normally associated with glassy liquids [1–4]. Their response to mechanical perturbations (shear, stress, strain) is a fascinating and poorly understood problem in nonequilibrium statistical mechanics. It is also an exceptionally important problem for technologically relevant processes [2,4]. For example, novel manufacturing schemes such as the robotically controlled direct write method employ dense particle suspensions ("inks") to fabricate three-dimensional hierarchically organized structures and devices [5]. Strain softening of the elastic modulus, stress- and shear-induced viscosity reduction, and static and dynamic yielding ("solid-to-fluid transition") are examples of phenomena of great interest. The relative role of mechanically driven structural rearrangements versus ultra slow thermally activated relaxation processes is a complex and material-specific issue.

New theoretical approaches to "soft glassy rheology" problems have appeared in recent years [1]. In the phenomenological and coarse-grained category, generic and minimalist "trap models" [6–8] have been developed and widely applied [9,10]. The elementary unit is usually a mesoscopic fluid region, and essential elements include a postulated distribution of barriers and noise-induced hopping transport out of locally harmonic traps. These are generally scalar models which for technical simplicity neglect the tensorial aspects of mechanical deformation. In a mean field spirit, nonlinearities before yielding are not taken into account since local strains are assumed to follow macroscopic strains and the shear rate is modeled as spatially homogeneous. Shear or strain reduces the barrier height for escaping a trap, and the distribution of trap energies is taken to be unaffected by mechanical perturbation. The latter simplification is of a "near equilibrium" nature since it effectively assumes the structure of the material is not significantly altered by strain or shear. Very recent work has taken a first step toward a full tensorial trap model for foams and emulsions [11]. The trap models are mathematically simple, and allow a generic and useful exploration of the rich nonlinear rheological possibilities for soft materials. A drawback is their strong phenomenological nature since a significant amount of the physics is "put in by hand" which limits quantitative and material-specific predictive ability [12].

Ambitious "first principles" microscopic theories for soft glassy rheology have been recently proposed which build on the ideal mode coupling theory (IMCT) of hard sphere colloidal suspensions [13–18] or related "schematic" dynamic mean field *p*-spin models [12,19]. These approaches are formulated in terms of static and dynamic two-point correlation functions. Fuchs and Cates [16,17] have employed projection operator techniques to derive a closed equation for the dynamic structure factor under steady flow. The tensorial nature of the shear deformation has been neglected resulting in an "isotropically sheared hard sphere model" (ISHSM) version [16,17] of IMCT. Velocity fluctuations are also not taken into account so that the microscopic shear flow is locally identical to the macroscopic one. Shear-induced acceleration of dynamics enters via the advection of cage scale fluctuations. In essence, shear separates particles at a rate $\dot{\gamma}$ which kinetically destroys or decorrelates the cage constraints encoded in the dynamic memory function [16,17]. This approach has also been worked out in a schematic form [13] where the wave vector dependence of vertices is ignored corresponding to a simplified description of local fluid structure [16,17].

*Corresponding author. Electronic address: kschweiz@uiuc.edu

Interesting results have been obtained based on the ISHSM and schematic versions of IMCT, which appear to be qualitatively identical to each other in most respects [16,17]. Noteworthy results include the prediction of shear thinning of the viscosity, a yield stress, and "melting" of the MCT ideal glass state at arbitrary small, but nonzero, shear rates. Some of these results agree with the alternative *p*-spin schematic dynamic mean field theory, and some do not [12]. In contrast to the trap model approach, barriers and activated hopping play no role. Moreover, as true for the corresponding quiescent problem, the nonlinear behavior is controlled by a "separation parameter" $\varepsilon \equiv (\phi - \phi_c)/\phi_c$ which quantifies the colloid volume fraction relative to the (hypothetical) ideal glass transition at a critical volume fraction ϕ_c.

Miyazaki and Reichman have independently constructed an ideal MCT for sheared colloidal suspensions [18]. It differs in several ways from the work of Refs. [16,17] including utilization of a shear distorted structure factor, a fluctuation-dissipation theorem, and a fluctuating hydrodynamics plus loop expansion method of derivation. Their final expression for the memory function in the presence of shear is *identical* to the quiescent equilibrium form except for the presence of a time-dependent wave vector associated with the advection of fluctuations.

Computer simulations have begun to address the problem of nonlinear dynamics of model glassy liquids [18–26]. Yamamoto and co-workers discovered the surprising and important result that the shear rate dependence of static correlations, and the anisotropy of particle diffusion and incoherent and coherent dynamic structure factors, is extremely small [21,22]. This is true even at high shear rates (in the shear thinning regime) where relaxation times and transport coefficients are dramatically affected. The various MCT theories [16–18,22] appear to be in rather good agreement with these simulations, and the inclusion of explicitly anisotropic structural correlations in the memory function does not significantly induce anisotropic dynamics [22]. All these studies provide strong support for the neglect of the tensorial aspect of the problem by trap model theories and the ISHSM version of MCT. One caveat is that the simulations have limitations regarding the degree of supercooling that can be studied, and are usually restricted to a "precursor" regime where the influence of high barriers and rare activated processes is not deeply probed. Interestingly, landscape analyses of the molecular dynamics simulations have suggested an alternative physical picture where shear strain causes the disappearance of potential energy minima and/or reduces barriers which then triggers modulus softening, shear thinning and enhanced diffusion via *irreversible* jumplike particle motions [24,25]. These studies claim the yielding process is akin to a *local* mechanical instability associated with the rearrangement of a small number of particles. The surprising ability of two totally different theoretical pictures, MCT versus barrier hopping, to qualitatively describe some aspects of the glassy shear thinning problem has been recently emphasized [22].

The trap models and IMCT type approaches are very different and have their own strengths and weaknesses. We believe simulations and experiments suggest that aspects of both are needed in order to construct a predictive microscopic theory of the nonlinear rheology of colloidal suspensions. Schweizer and Saltzman recently built on a simple version of ideal MCT for quiescent colloidal suspensions to "go beyond" the mode coupling approach and treat entropic barrier formation and activated transport [27,28]. An ideal glass transition plays no role. Dynamical slowing down is a continuous, albeit precipitous, process with increasing colloid volume fraction. The no adjustable parameter comparisons of the theoretical predictions for various single particle dynamical properties and transport coefficients were found to be in good agreement with the experiment. A physical picture is suggested where there is no dynamic critical point and entropic barrier hopping is responsible for the dramatic slowing down in the high volume fraction regime. Interestingly, recent simulation studies [29,30] of both thermal and hard sphere glass forming liquids find that activated barrier hopping does appear to commence close to the theoretically predicted MCT dynamic critical point (temperature or volume fraction), and is dominant in the system parameter range commonly associated with precursor supercooled or glassy dynamics. These findings are in qualitative accord with our theoretical work [27,28].

The purpose of this paper is to generalize the beyond MCT approach [27,28] to treat glassy nonlinear rheological phenomena. In Sec. II the theory for quiescent hard sphere colloidal suspensions is reviewed, and calculations of the elastic shear modulus are presented and compared with the experiment. Generalization of the theory to treat the consequences of external stress, strain and shear is given in Sec. III, and numerical calculations for the dependence of various features of a "nonequilibrium" free energy on mechanical perturbation are presented. The theory is applied to glassy suspensions in the absence and presence of activated barrier hopping in Secs. IV and V, respectively. Multiple model calculations are presented and compared with the experiment. Some results are also contrasted with IMCT and related approaches. The paper concludes in Sec. VI with a summary and discussion.

II. THEORY OF ENTROPIC BARRIERS AND ACTIVATED HOPPING

The entropic barrier hopping theory has been described in detail elsewhere [27,28]. Here the essential elements are recalled.

A. Basics

The "naive" version of idealized mode coupling theory of Kirkpatrick and Wolynes [31] focuses on the dynamics of a tagged particle. The central object is the force-force time correlation function, or dynamic friction, due to the surrounding fluid

$$K(t) = \langle \vec{F}(0) \cdot \vec{F}(t) \rangle = \frac{1}{3}\beta^{-2} \int \frac{d\vec{q}}{(2\pi)^3} q^2 C^2(q) \rho S(q) \Gamma_s(q,t) \Gamma_c(q,t). \quad (1)$$

Here ρ is the particle number density, $\vec{F}(t)$ is the force ex-

erted on a particle by the fluid at time t, and β is the inverse thermal energy. $C(q)$ is the Fourier transform of the direct correlation function and $S(q)$ the dimensionless collective structure factor, which are calculated in the present work using Percus-Yevick (PY) integral equation theory [32]. The propagator $\Gamma_S(q,t)[\Gamma_C(q,t)]$ is the $t=0$ normalized single particle (collective) dynamic structure factor which in fluids decays to zero at long times, but is nonzero in a glass. The long time nonzero values of the propagators (Debye-Waller factors) describe localized single particle and collective density fluctuations in a harmonic or Einstein model of an amorphous solid [27,31]:

$$\Gamma_S(q,t\to\infty)=e^{-q^2/4\alpha},\quad \Gamma_c(q,t\to\infty)=e^{q^2/4\alpha S(q)}. \tag{2}$$

A standard ensemble averaged localization length [31] is the local order parameter and it is defined as

$$r_L^2\equiv\langle r^2\rangle=3/2\alpha. \tag{3}$$

Derivation of a self-consistent equation for the dynamic order parameter is straightforward [27,31],

$$\alpha=\frac{1}{2}\beta^2K(t\to\infty)=\frac{1}{6}\int\frac{d\vec{q}}{(2\pi)^3}\rho q^2C^2(q)S(q)e^{-(q^2/4\alpha)[1+S^{-1}(q)]}. \tag{4}$$

Based on PY theory input, a localization transition occurs at a fluid volume fraction $\phi_{MCT}\equiv\phi_c=0.432$ which corresponds to the naive IMCT glass transition and lies below the full IMCT value [13] of 0.515 based on PY input.

To treat barriers and activated events, the IMCT nonergodicity transition is interpreted as signaling *transient* localization and the emergence of finite barriers in a *dynamically defined* landscape. To move beyond MCT a stochastic equation of motion (EOM) is constructed for the single particle *dynamical order parameter*, $r(t)$, the non ensemble averaged *displacement* from a randomly located initial position. This reduced dynamical description is in the spirit of Kramers' theory of activated processes or a Zwanzig-Kawasaki projection operator derivation of a nonlinear Langevin equation. However, as previously emphasized [27] the theory was not rigorously derived. A nonlinear, stochastic Langevin equation is constructed guided by three ideas [27]. (i) Brownian colloids move by Fickian diffusion at short times. (ii) IMCT is assumed to correctly predict the tendency to localize in a cage in the absence of a certain type of thermal fluctuations or noise. In the deterministic limit the EOM is required to recover the naive IMCT localization condition. This idea guides the construction of a *displacement-dependent* effective caging *force* $-\partial F/\partial r$, which favors localization at high particle volume fractions. F is called an "effective" or "nonequilibrium" free energy functional, although it does not have any rigorous equilibrium meaning and depends on $r^2(t)\equiv 3/2\alpha(t)$. (iii) Ergodicity restoring thermal noise destroys the naive IMCT glass transition and allows for activated hopping when $\phi>\phi_C$. The resulting nonlinear Langevin equation in the overdamped limit corresponds to a force balance [27]

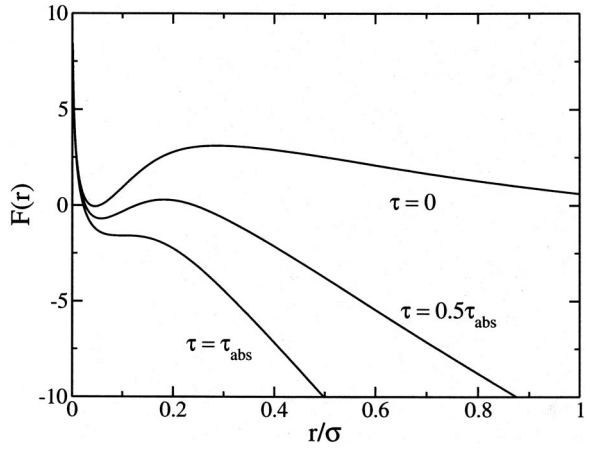

FIG. 1. "Nonequilibrium free energy" or entropic trapping potential (in units of k_BT) as a function of reduced colloid displacement at a volume fraction of $\phi=0.53$ for zero stress, the absolute yield stress, and one-half the absolute yield stress.

$$-\zeta_s\frac{d}{dt}r-\frac{\partial}{\partial r}F+\delta f=M\frac{d^2}{dt^2}r=0, \tag{5}$$

where ζ_S is a short time friction constant due to two-particle hydrodynamic interactions [4] or independent binary collisions [32,33]. Based on the latter,

$$\zeta_s=\zeta_0g(\sigma),\quad \zeta_0=k_BT/D_0=3\pi\sigma\eta_0, \tag{6}$$

where η_0 is the solvent viscosity, and $g(\sigma)$ is the contact value of the radial distribution function [27,33]. The use of two-particle hydrodynamics to quantify the short time friction constant has been shown to yield results nearly identical to the binary collision approach [27]. The white noise fluctuating force in Eq. (5) is statistically uncorrelated with the tagged particle position and velocity and satisfies $\langle\delta f(0)\delta f(t)\rangle=6\beta^{-1}\zeta_s\delta(t)$.

An alternative motivation of Eq. (5) is to view $r(t)$ as a coarse-grained and/or partially ensemble-averaged dynamic order parameter. Then Eq. (5) is of a time-dependent Landau-Ginzburg form or model A of dynamic critical phenomena [34], in the sense that the rate of change of the dynamic order parameter is proportional to a "thermodynamic like" force which for the glassy dynamics problem is of nonequilibrium origin. In this interpretation, the random noise in Eq. (5) is present to avoid trapping in a metastable state [34], which for our problem is the MCT ideal glass corresponding to the local minimum of $F(r)$ (see Fig. 1).

The crucial quantity in Eq. (5) is the "nonequilibrium" free energy (in units of k_BT), whose gradient quantifies the transient caging force. It is constructed in the spirit of density functional theory (DFT) [35] where $F(\alpha)$ describes the difference between localized (nonzero α) and delocalized ($\alpha=0$) states. The apparently deep connection between an equilibrium DFT and an explicit time-dependent treatment of glassy dynamics is the central idea of the work of Kirkpatrick and Wolynes [31], and motivates the explicit result [27]

$$F(\alpha) = \frac{3}{2}\ln(\alpha) - \int \frac{d\vec{q}}{(2\pi)^3}\rho C^2(q)S(q) \times [1 + S^{-1}(q)]^{-1} e^{-(q^2/4\alpha)[1+S^{-1}(q)]} \equiv F_0 + F_I. \quad (7)$$

The leading "ideal" term favors the fluid state as in DFT for a *strongly localized* harmonic solid. The second "interaction" contribution corresponds to an entropic trapping potential favoring localization. Minimization of Eq. (7) with respect to α, or solution of Eq. (5) in the absence of noise, *by construction* yields the naive IMCT localization condition of Eq. (4). For $\phi > \phi_c$, an entropic barrier of magnitude F_B emerges in $F(r)$ as shown in Fig. 1. Characteristic length scales include the location of the minimum ("localization length" r_L as in IMCT), the displacement corresponding to maximum restoring (caging) force R^*, and the local maximum (barrier location) r_B. Both the localization length and displacement of maximum restoring force are small ($\ll\sigma$), and decrease strongly with colloid volume fraction as $r_L/\sigma \sim 30\exp(-12.2\phi)$ and $R^*/\sigma \sim \exp(-6.6\phi)$ [27]. The barrier location increases weakly with volume fraction varying from $\sim 0.25\sigma$ to 0.4σ as ϕ increases from 0.5 to 0.62 [27]. As discussed previously [27], for the sole purpose of calculating transport coefficients a "diffusion length" L_D is introduced and defined as the displacement beyond which the interaction part of the force, $-\partial F_I/\partial r$, is negligible and Fickian diffusion is recovered. Calculations find L_D is nearly ϕ independent and $\approx 0.8\sigma$ [27].

The caging force in Eqs. (5) and (7) evolves in time via single particle and collective motions. However, collective motion is treated within a simplified Vineyard type approximation [32] for the collective propagator which neglects explicitly many particle dynamics. Such an approximation is known to be quite accurate on the local cage scales [31,32] of present interest. It is in this sense that the approach is a dynamical mean field theory. The caging force is self-consistently and nonlinearly coupled with single particle motion. Hence, for hopping transport Garrahan has suggested the theory might be interpretable as containing some aspects of the "dynamic facilitation" idea in the sense that the evolution of the dynamic order parameter is state (displacement) dependent [36].

The *mean* barrier hopping time τ_{hop} is expected to be closely correlated with the α or structural relaxation time. In the overdamped, high friction limit barrier crossing is a diffusive process and Kramers' theory [37] yields [27]

$$\frac{\tau_{hop}}{\tau_0} = \frac{2\pi g(\sigma)}{\sqrt{K_0 K_B}} e^{F_B}, \quad (8)$$

where $\tau_0 = \sigma^2\zeta_0/k_BT$ is the elementary Brownian diffusion time, and K_0 and K_B are the absolute magnitudes of the harmonic curvatures of the minimum and barrier of $F(r)$, respectively.

A few additional comments concerning the conceptual basis and range of technical applicability of the theory are worth making. The former involves the level of coarse graining assumed and the meaning of ensemble averages. It is well known that MCT is not valid at very short times or length scales since it is meant to capture the slow, longer time collective aspects of caging [13]. In this sense, given that our starting point is MCT, a small amount of space and time coarse-graining is invoked and the missing physics is buried in the short time friction constant in Eq. (6). Based on the Langevin and Kramers' theory motivation for the construction of our nonlinear stochastic equation of motion, $r(t)$ is a non-ensemble-averaged dynamic variable (to within the aforementioned short time/distance coarse-graining caveat). However, the caging force is constructed using DFT-like ideas that relate the inhomogeneous system (analog of the dynamically localized state) to the homogenous system. Thus, ensemble-averaged structural information **(**$S(q), C(q)$**)** is employed to quantify the effective caging force in Eq. (5). In the aforementioned model-*A*-like interpretation of Eq. (5) the dynamic order parameter $r(t)$ is also coarse-grained and remains stochastic due to the random force term.

The technical applicability question relates to the range of validity of the "free energy" of Eq. (7) with regard to dynamic displacements. As discussed previously [27], our goal (for both the quiescent and deformed systems) is restricted to the elementary *dynamical* process of transient localization and barrier hopping. $F(r)$ in Eq. (7) does not have a rigorous equilibrium meaning, and additive constants that arise in its equilibrium DFT analog have been dropped. A strong localization approximation has been employed to construct the ideal contribution $F_0(r)$, which is the origin of unphysical divergence to negative infinity of $F(r) \to -\infty$ as $r \to \infty$. A more accurate treatment of $F_0(r)$ is possible within a thermodynamic DFT framework [38]; however, for displacements $r < \sigma/2$ the far simpler Eq. (7) is accurate [38]. Given that our interest is restricted to the elementary localization and hopping processes, where the relevant displacements (r_L, R^*, r_B) are *all smaller* than $\sigma/2$, any errors incurred by using the strong localization form of the ideal free energy should be minor. Finally, after completion of this manuscript an explicit derivation of the beyond MCT approach using dynamic density functional ideas has been achieved [39].

B. Transport coefficients and elastic shear modulus

Transport coefficients are calculated using Green-Kubo formulas and the MCT factorization of multipoint correlations approximation [13,32]. The dynamic propagators are determined using a generalization of the "binary collision in a mean field" (BCMF) theory [33] to include an activated barrier hopping contribution to the friction constant. The resulting shear viscosity is [28,33]

$$\eta = \eta_\infty + \frac{k_BT}{120\pi^2}\int_0^\infty dq\, q^2\left(\frac{\partial}{\partial q}\ln S(q)\right)^2 \frac{1}{D_s^c(q)} \quad (9)$$

where the high frequency viscosity is $\eta_\infty = \eta_0 g(\sigma)$. The cage diffusion constant is

$$D_c^s(q) = \frac{D_0}{S(q)[g(\sigma)d(q)^{-1} + (\zeta_{hop}/\zeta_0)]}, \quad (10)$$

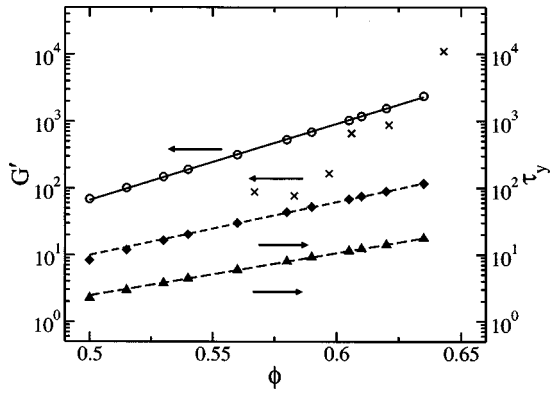

FIG. 2. Elastic modulus and yield stress (both in units of k_BT/σ^3) as functions of volume fraction. Open circles are the elastic modulus at zero stress, and crosses are the corresponding linear response experimental data of Petekidis *et al.* [43]. Solid diamonds are the absolute yield stress, and solid triangles the stress at which the elastic modulus drops by 10% (perturbative yield). Lines are exponential fits discussed in the text.

$$d(q) = [1 - j_0(k\sigma) + 2j_2(k\sigma)]^{-1}, \tag{11}$$

where j_k is the spherical Bessel function of order k. The total friction constant is taken to be the sum of short time [Eq. (6)] and hopping contributions [28],

$$\zeta_{hop} = k_BT/D_{hop} = 6k_BT\tau_{hop}/L_D^2 = 6\zeta_0\frac{\tau_{hop}}{\tau_0}\tilde{L}_D^{-2}, \tag{12}$$

where L_D was defined below Eq. (7) and is $\sim 0.8\sigma$ [40]. For $\phi < \phi_c$, Eqs. (9)–(11) correspond to the BCMF theory which is accurate in the "normal fluid" regime ($\phi < 0.45$–0.5) where $\eta/\eta_0 \leqslant 20$–30 [33]. For $\phi > \phi_c$, the no adjustable parameter calculations of the localization length, single particle relaxation time, viscosity, diffusion constant, and other quantities are in good agreement with experiments over the entire volume fraction regime probed experimentally (up to $\phi \sim 0.56$–0.58) [27,28].

The elastic modulus is computed using the standard Green-Kubo formula [12,32]:

$$G' = \frac{k_BT}{60\pi^2}\int_0^\infty dq\left(q^2\frac{\partial}{\partial q}\ln S(q)\right)^2 e^{-q^2/2S(q)\alpha} \tag{13}$$

where the localization parameter α is given by Eq. (4). This is the naive version of the IMCT glassy shear modulus. Calculations of elastic modulus based on PY structural input are shown in Fig. 2. An exponential volume fraction dependence is found:

$$G' = 0.000\ 16\frac{k_BT}{\sigma^3}e^{26\phi}. \tag{14}$$

Since the localization length has been previously shown to be [27]

$$r_L \cong 30e^{-12.2\phi}\sigma, \tag{15}$$

a direct relation between it and the elastic modulus is implied:

$$G' \cong 0.144\frac{k_BT}{\sigma^3}\left(\frac{\sigma}{r_L}\right)^{2.13}. \tag{16}$$

A nearly identical relationship between G' and the localization length has been suggested based on elementary mechanics arguments [41], and was also found theoretically for depletion gels [42]. The modulus calculations can alternatively be well fitted over the range $\phi \sim 0.5$–0.65 by a power law with a high exponent, $G' \propto \phi^{14}$.

Recent experimental results [43] for G' of hard sphere suspensions at very high volume fractions are shown in Fig. 2. Given the difficulties of the experiments and moderate polydispersity of the samples, the no adjustable parameter calculations seem reasonable. Moreover, multiple prior experimental studies of (near) hard sphere suspensions have repeatedly reported exponential behavior [44–46], $G' \propto \exp(b\phi)$. The absolute magnitudes of G' and the b values are variable given the common experimental difficulty in precisely defining an effective hard sphere volume fraction, and particle "hardness" differences due to variable grafted polymer layers or the presence of charge. For example, $b \sim 9$ for silica with long polydimethylsiloxane polymer grafts [46], $b \sim 28$ for polymethylmethacrylate colloids with short grafts [46], and $b \sim 28$ for $\phi \sim 0.4$–0.6 charge stabilized near hard sphere suspensions [44]. For the short-range repulsion systems, the measured values of b are remarkably close to the theoretical value of 26. There have also been reports [46] of G' scaling with ϕ as a high exponent power law, $G' \propto \phi^{10\pm1}$. The absolute value of the experimental moduli are often in semiquantitative accord with our calculations, especially for "simple" particles. For example, $G' \sim 10$ Pa for room temperature suspensions of $\phi = 420$ nm bare silica hard spheres [47] at $\phi = 0.56$ which can be compared with the theoretical value of ~ 16 Pa.

III. GENERALIZATION TO MECHANICALLY DEFORMED SYSTEMS

A. Theory formulation

Our generalization to nonlinear response is motivated by a desire for technical simplicity and several facts established by experiments and computer simulations. Watanabe *et al.* [48] and Manzano and Wagner [49] studied the nonlinear rheology and collective structure factor of model silica *hard sphere* suspensions. Surprisingly, strong nonlinear dynamical effects such as strain softening of the modulus and shear thinning of the viscosity are *not* accompanied by significant anisotropy of structure in the *shear thinning* regime. Up to volume fractions of 0.5, no significant changes in $S(q)$ are observed in the presence of shear [49]. At very high shear rates where (presumably) hydrodynamically driven shear thickening occurs, anisotropy of the structure factor does emerge, and this regime is not treatable in our approach. As mentioned in the Introduction, simulations of liquids (no hydrodynamic interactions) [20–23] also find that even for shear rates where the viscosity is strongly thinning (up to $\dot{\gamma}\tau_\alpha \sim 10^3$ where τ_α is the quiescent α relaxation time) and self-diffusion is enhanced, the particle mean square displacements (in the advected frame), intermolecular radial distribu-

tion functions, structure factor various relaxation times, and wave-vector-dependent dynamic structure factors remain nearly isotropic. Hence, experiment and simulation both find anisotropic shear perturbations induce much faster dynamics in a surprisingly isotropic manner in the shear thinning regime. In addition, simulations find [21,22] that the shear-induced reduction of single particle and collective relaxation times is nearly length scale independent for wave vectors that probe cage scale dynamics.

To model how an external deformation modifies Eqs. (5) and (7) we adopt the simplest idea that a constant applied stress results in a constant (scalar) force f on the tagged particle. The effective nonequilibrium free energy is thus modified as

$$F(r) = F(r;\tau = 0) - fr. \tag{17}$$

In analogy with prior theoretical studies [9–12,16,17], the macroscopic deformation is assumed to be transmitted to the particle level. This description is in the spirit of a "single particle" trap model approach [9] where the local strain is envisioned to induce a relative displacement of a colloid from the center of its cage formed by the surrounding particles. However, given possible complications in real materials associated with the transmission of a macroscopic stress to the microscopic scale [50], a unique quantitative connection between the microscopic force f and the macroscopic stress τ cannot be simply written. We proceed to make the connection via physical arguments.

In static equilibrium (before yield), stress is assumed to be constant throughout the material. This implies that the microscopic stress τ_{micro} equals the macroscopic force τ_{macro} acting on the unit cross section of the particle network, reduced by the average area occupied by particles in the unit cross section, $\tau_{micro} = \tau_{macro}/\phi^{2/3}$. This implies that the average external force on a particle is

$$f_{micro} = \langle \tau_{micro} A \rangle = \tau_{macro} \langle A \rangle / \phi^{2/3}, \tag{18}$$

where A is the relevant particle cross sectional area which can be estimated in several ways. One estimate is the total area occupied by particles divided by the number of particles, which yields $\langle A \rangle = \phi^{2/3}/\rho^{2/3}$, resulting in

$$f_{micro} = \left(\frac{\pi}{6}\right)^{2/3} \sigma^2 \frac{\tau_{macro}}{\phi^{2/3}}. \tag{19}$$

Alternatively, assuming $\langle A \rangle$ equals the average cross sectional area of the spherical particle yields

$$f_{micro} = \frac{\pi}{6} \sigma^2 \frac{\tau_{macro}}{\phi^{2/3}}. \tag{20}$$

There is no rigorous justification of either choice, and no doubt there are alternative arguments that yield qualitatively the same connection between microscopic force and macroscopic stress. The basic form of the above connections assume that virtually all stress is borne by the particle network, not the continuous solvent phase, an assumption that is expected to be accurate at the very high volume fractions of interest [50]. Hence, we simply parametrize the *constant numerical prefactor* uncertainty and write

$$f_{micro} = \lambda \sigma^2 \frac{\tau}{\phi^{2/3}}, \tag{21}$$

where λ is of order unity. All calculations, figures, and discussion of numerical results presented are based on $\lambda = 1$. For alternative choices of λ the quoted stress, strain, and shear rate are simply modified by the factor of λ^{-1}.

The final expression for the nonequilibrium free energy (in $k_B T/\sigma^3$ units) is

$$F(\alpha) = \frac{3}{2}\ln(\alpha) - \int \frac{d\vec{q}}{(2\pi)^3} \rho C^2(q) S(q) \times [1 + S^{-1}(q)]^{-1} e^{(q^2/4\alpha)[1+S^{-1}(q)]} - \frac{\tau}{\phi^{2/3}} \sqrt{3/2\alpha}. \tag{22}$$

Here, and throughout the paper, the unit of length is σ and the stress is given in units of $k_B T/\sigma^3$. Equations (17)–(22) account for the effect of applied stress at the simplest "one-body," or external-field-like, level. Of course, steady shear does convect particles and changes their relative separation with time [16–18]. In MCT this is the "advection of fluctuations" effect which enters at the two-point time correlation function level. However, in the steady state situation of interest, the shear rate and constant stress modes of deformation are equivalent [2]. In the strain mode of deformation, there will be strain-driven relative displacements of pairs of particles which in principle induce anisotropy in the radial distribution function and structure factor. These are assumed to be small "higher order" effects, and the same quiescent equilibrium correlation functions are employed to quantify the cage constraints and $F(r)$. The usefulness of such a simplification is buttressed by the fact that we find that the absolute yield point is associated with relatively small strains and particle displacements. Ignoring deformation-induced changes in our "trap potential" $F(r)$ is also in the spirit of the phenomenological glassy soft rheology approaches [9,10].

Applied shear, stress, or strain distorts the effective free energy function and reduces the barrier leading to more rapid Brownian dynamics. In the stress-controlled mode τ is fixed, and $G'(\tau)$ is directly computed from Eq. (13). The corresponding dimensionless strain γ follows from the generic nonlinear stress-strain relation [2]:

$$\gamma = \tau / G'(\tau). \tag{23}$$

The absolute yield stress τ_{abs} is the minimum stress required to destroy the barrier in $F(r)$. This is equivalent to the condition that the applied force is equal and opposite to the maximum cage restoring force of the quiescent system. Since the displacement corresponding to the latter, R^*, is much smaller than σ [27], the strong localization form of $F_0(r)$ is reasonable. An example of the consequences of applied stress on $F(r)$ is shown in Fig. 1. In the absence of barrier hopping, the absolute yield stress defines a solid-to-liquid, or mechanical yield, transition. For a strain-controlled experiment, Eq. (23) is solved in an iterative self-consistent manner. For the shear-rate-controlled experiment, the appropriate shear rate follows from the defining relation [2]

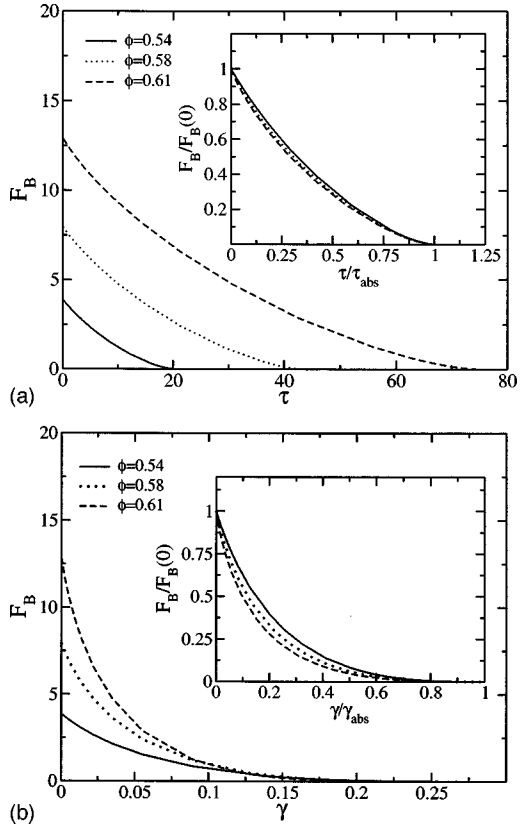

FIG. 3. (a) Entropic barrier height (in units of k_BT) as a function of stress for three volume fractions. The inset shows the same results with the barrier height normalized by its zero stress value and the stress normalized by the absolute yield stress. (b) Same as (a) but as a function of strain. Double normalized plots are shown in the inset.

$$\tau = \dot{\gamma}\eta(\tau). \tag{24}$$

Finally, as in the quiescent case [27], we again emphasize that the large r dependence of $F(r)$ is not relevant given our limited focus on the preyield, small displacement regime.

B. Strain and stress dependence of the nonequilibrium free energy

Applied stress or strain induces distinctive changes of the characteristic length and energy scales in *F(r)* which are summarized in Figs. 3–5. Figure 3(a) shows that the barrier is reduced nonlinearly with increasing stress, in a manner qualitatively in accord with the computer simulation landscape analyses [24,25]. The inset shows that nondimensionalization of the barrier by its zero stress value, and the stress by the absolute yield stress, results in a nearly universal behavior. The analogous results based on strain as the mechanical control variable are given in Fig. 3(b). The barrier is largely destroyed beyond a dimensionless strain of 15–20 %. However, its strain dependence is different from the stress dependence, and the inset shows that nondimensionalization does not result in as good a collapse.

The dependence of the localization and barrier length scales on stress and strain are presented in Fig. 4. The unperturbed localization (barrier) length decreases (increases) with ϕ. Physically one expects $r_L \to 0$ as the volume fraction approaches the incompressible random close packing state ($\phi \sim 0.63$) [51]. Its failure to do so is a limitation of PY theory for $S(q)$. With increasing stress, these length scales approach each other in a nonlinear fashion and merge at the absolute yield stress. The strain dependence shown in the inset is similar, although interestingly the localization length is a nearly linear function of strain up to the mechanical yield point. The calculated strain or stress enhancement of the localization length might be relevant to recent attempts to use the diffusing wave light scattering echo technique to estimate strain-induced colloidal displacements [43].

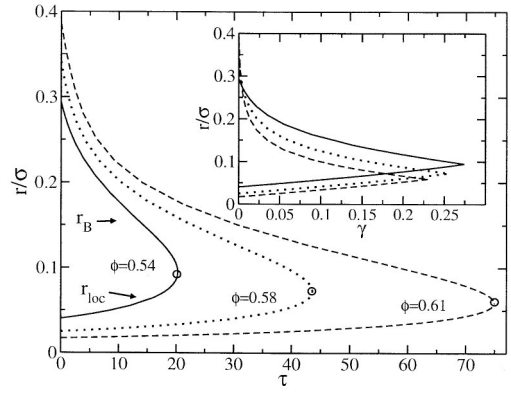

FIG. 4. Localization length (lower curves) and barrier location (upper curves) as a function of stress (main panel) or strain (inset) for different volume fractions. Open circles correspond to the absolute yield point where the barrier disappears and the two lengths coincide.

The strain and volume fraction dependence of the well and barrier curvatures are presented in Fig. 5. The well curvature controls the vibrational amplitude and oscillation frequency in the (quasi)localized state. It decreases monotonically with strain and (nearly linearly) with stress. In contrast, the barrier curvature initially increases in magnitude with strain or stress before ultimately decreasing to zero at the

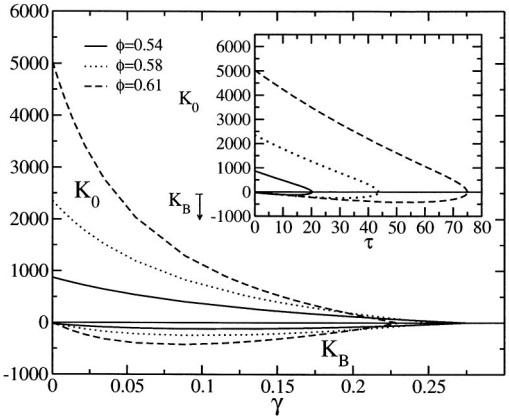

FIG. 5. Curvatures (units of $k_BT\sigma^{-2}$) at the minimum (K_0) and barrier (K_B) of $F(r)$ as a function of strain for different volume fractions. The corresponding stress dependence is shown in the inset.

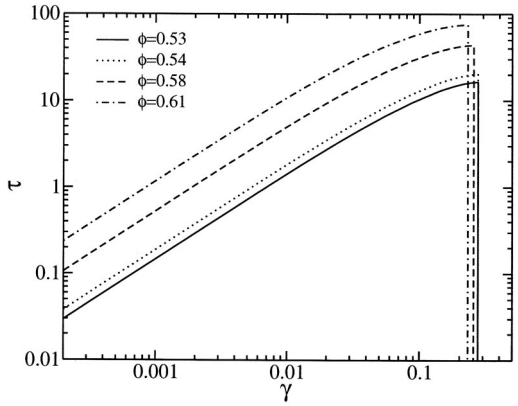

FIG. 6. Stress-strain relation at different volume fractions. The discontinuous drop of the stress to zero defines the absolute yield point.

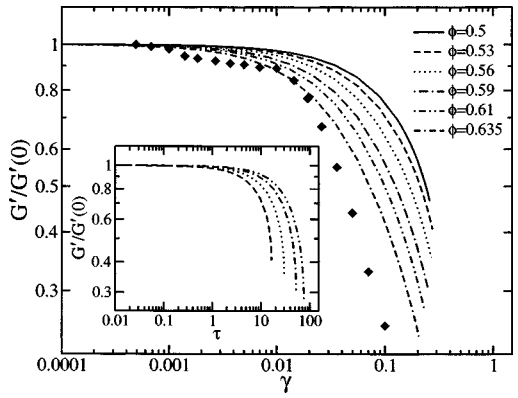

FIG. 7. Ratio of the elastic modulus to its linear response value as a function of strain for different volume fractions. Symbols are experimental data by Petekidis *et al.* [40]. The inset shows the corresponding stress dependence.

yield stress or strain. The rich dependence of all the features of $F(r)$, on stress, strain, and volume fraction is relevant to the prediction of the hopping time and transport coefficients.

IV. MECHANICALLY DRIVEN REGIME

In this section the predictions of our theory in the absence of barrier hopping are worked out. This is the naive MCT limit where the noise term in Eq. (5) is dropped. As in the quiescent state, delocalization and flow occur when the local minimum and barrier in $F(r)$ disappear. For $\phi > \phi_c$, this condition requires an external mechanical force and first occurs, by definition, at a critical, or absolute yield stress or strain. Our results are the nonlinear version of the naive IMCT ideal glass transition condition, and hence will be compared to recent efforts to generalize the full IMCT to nonlinear rheology [16–18,22]. Any differences between the predictions of our approach and prior ideal MCT work reflects both our simplification of the full IMCT to its naive version, and the manner in which the external deformation is incorporated. The neglect of activated hopping in this section suggests quantitative theoretical results for the yield stress and strain should be upper bounds to the true (barrier hopping influenced) behavior. The latter kinetic aspect is examined in Sec. V where the dynamic yield stress is contrasted with its static analog. Of course, given the unknown quantitative accuracy of prior IMCT work and our present theory the issue of whether the numerical results of this section are true upper bounds for experimental systems cannot be definitively known. Note that our analysis does not apply to literal $T=0$ non-Brownian or granular systems.

Figure 6 shows representative results for the stress-strain curve. Linear response occurs for strains up to a characteristic value beyond which the material continuously softens until the yield point is reached. The dimensionless absolute yield stress is given in Fig. 2 and is a strongly increasing function of volume fraction. It varies from ~10 to 100 as volume fraction increases from ~0.52 to 0.63. The yield stress is well described by an exponential law with a slope that is smaller than found for the linear elastic shear modulus G' in Eq. (14), $\tau_{abs} \propto \exp(19.2\phi)$. A power law dependence with a high exponent, $\tau_{abs} \sim 17\,200\phi^{11}$, also provides an excellent fit (not shown). Following common experimental practice [2,4], a perturbative yield stress is defined as the stress at which the linear elastic modulus is reduced by 10%. As seen in Fig. 2, $\tau_{pert} \sim 880\phi^{8.6}$ which corresponds to a modestly weaker growth with ϕ than the absolute yield stress.

Experiments [46] on hard-sphere-like suspensions at high volume fractions find the yield stress grows as a power law with an exponent ~9–11. Recent rheological creep recovery measurements [43] on colloidal glasses composed of particles of diameter 366 nm find the absolute yield stresses are ~4–12 Pa for $\phi \sim 0.59$–0.62. The results in Fig. 2 correspond to yield stresses of ~5–9 Pa for these volume fractions, in apparent remarkably good agreement.

Some aspects of our yield stress results can be compared with the ISHSM version of ideal MCT [16] which predicts $\tau_{crit} = 6(k_B T/\sigma^3)$ at the MCT critical volume fraction of $\phi_c \approx 0.515$ based on PY static input. Curiously, this value of yield stress is rather close to our result of ~12 at $\phi \sim 0.515$. At the experimental *kinetic* glass transition volume fraction of ~0.57–0.58, our theory predicts a dimensionless yield stress of ~30. With increasing volume fraction, the IMCT yield stress grows initially in a square root manner [16,17] $\tau_y - \tau_{crit} \cong 112\sqrt{\phi - \phi_c}$, in contrast with the exponential or high power law dependence of our theory. This implies any apparent near quantitative agreement between the numbers predicted by the two approaches cannot exist over a wide volume fraction range. Our prior work on the linear dynamics of hard sphere suspensions also found some intriguing similarities between the entropic barrier hopping approach and IMCT [27,28]. We note that schematic IMCT makes the same qualitative predictions for yield stress volume fraction dependence as the full ISHSM based theory [16,17].

The strain and stress dependence of the elastic modulus is shown in Fig. 7. Modulus softening occurs at lower strain amplitudes for denser materials. The functional dependence of G' on strain is gentle, and locally might be characterized as logarithmic. Petekidis *et al.* [43] have recently measured the strain dependence of the elastic modulus for very high

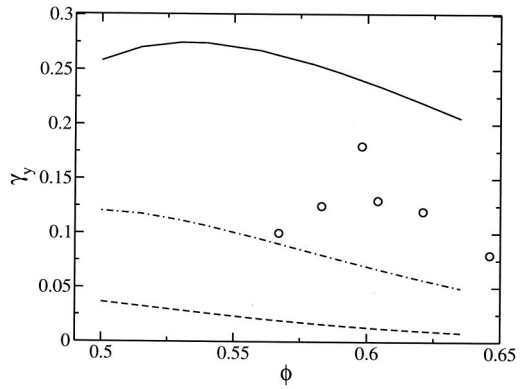

FIG. 8. Yield strain as a function of volume fraction. Solid curve is the absolute yield, dashed curve is the perturbative yield, and dash-dotted curve is a "mixed" yield strain defined as $\tau_{abs}/G'(0)$. The symbols are rheological data by Petekidis *et al.* [43].

volume fraction glassy colloidal suspensions ($\phi \approx 0.645$). They find, for example, that G' is reduced by a factor of roughly 4 at a strain of ~10%. A detailed comparison of theory with this experiment is shown in Fig. 7. The theoretical calculations are in reasonable agreement with the data.

The stress dependence of the elastic modulus is shown in the inset of Fig. 7, and is considerably stronger than the strain dependence. The transition from the onset of discernable softening to absolute yielding occurs over less than an order of magnitude in stress.

Figure 8 summarizes three measures of yield strain as a function of colloid volume fraction. The yield strain displays an extremely *weak* dependence on ϕ relative to the many orders of magnitude change in the yield stress and modulus. This implies the yield stress and shear modulus have similar volume fraction dependences, a trend observed in many experiments [44–46,52–54]. For $\phi > 0.53$, all measures of the yield strain decrease with volume fraction implying denser materials are "more brittle" in a strain mode of deformation.

The absolute yield strain in Fig. 8 is computed using the absolute yield stress and the nonlinear elastic modulus, and varies over the narrow range of ~20–27 %. Interestingly, it is predicted to be a *nonmonotonic* function of volume fraction. This numerically arises from Eq. (23) as a consequence of the subtly different dependences of yield stress and modulus on ϕ. One interpretation of the two competing processes which underlie this nonmonotonic dependence is as follows. With increasing volume fraction particles reside in deeper entropic wells with larger cage restoring forces (at $r = R^*$). However, the elastic modulus also strongly increases with volume fraction due to tighter localization (smaller r_L) which correlates with the modulus roughly as $G' \propto r_L^{-2}$. Given that the strain is a ratio of stress to modulus our numerical results suggest the maximum restoring force is decreased more strongly with strain than r_L is at very high volume fractions.

Recent mechanical creep measurements [43] of the yield strain of model hard sphere glasses is shown in Fig. 8. The absolute magnitude and gross qualitative shape are consistent with the calculations. Qualitatively identical results are found based on light scattering echo experiments [43] which probe the onset of irreversible colloid motion. We note that Chow and Zukoski [53] observed some time ago a nonmonotonic yield strain for dense charged stabilized suspensions with a maximum strain at $\phi \sim 0.5$.

The perturbative yield strain is defined as when the elastic modulus has decreased by 10%. Our calculations find it is much smaller than the absolute yield strain, lying in the range ~0.8–3.6 %, and decreases monotonically with volume fraction. A third "mixed" measure of a yield strain, often employed by experimentalists, is computed as the ratio of the absolute yield stress to the linear modulus. Results in Fig. 8 show that this yield strain is also a monotonically decreasing function of ϕ and varies over the range ~5–12 %. There have been many measurements of the yield strain for near hard sphere suspensions at high volume fractions and also for charged latex materials [44,46,52]. Remarkably, all these studies find perturbative or "mixed" yield strains in the relatively narrow range of ~1–5 %, often with little or no systematic dependence on ϕ. Globally, these observations are consistent with our calculations. It is also interesting to note that the typical perturbative or mixed yield strain for vastly different materials is similar, for example ~2–4 % for amorphous metals [55] and ~3–7 % for dense depletion gels [2,4,56,57].

Recent IMCT calculations [16] based on the ISHSM or schematic versions obtain a ("mixed") yield strain of $\tau_y/G'(0) \sim 0.33$ at the MCT critical volume fraction. This value is larger than the experimental results discussed above, or the ~5–12 % our theory predicts for $\phi \sim 0.52$–0.62.

Finally, numerical calculations reveal an interesting connection between our computed absolute yield strain γ_{abs} and the strain-induced increase of the localization length at the absolute yield point $\Delta r_{loc} \equiv r_{loc}(\gamma_{abs}) - r_{loc}(0)$. The ratio $\Delta r_{loc}/\gamma_{abs} \approx 0.18$ and is nearly volume fraction independent in the $\phi = 0.53$–0.63 regime, thereby implying a direct connection between strain and location of the minimum in $F(r)$. Such "universality" is reminiscent of the empirical "Lindeman criterion" $r_{loc}(0)/\sigma \approx 0.15$, for the fluid-crystal phase transition [32] and the ideal glass transition of MCT [13,31]. However, the strain aspect has no analog in the latter two phenomena. Rather, the near constancy of $\Delta r_{loc}/\gamma_{abs}$ can be qualitatively understood as a consequence of the predicted close relationship between the localization length and harmonic curvature (K_0) of $F(r)$, or equivalently a nonequilibrium equipartition relation, as previously discussed for quiescent colloidal glasses [27] and gels [42]. Specifically, it was shown [27,42] that $K_0 \propto r_{loc}^{-2} \propto G'$, which for a harmonic $F(r)$ implies a strain-induced *shift* of the localization length $\Delta r_{loc} \propto \tau/K_0 \propto \tau/G' \propto \gamma$. The fact that $\Delta r_{loc}/\gamma_{abs}$ remains essentially constant for stresses up to the yield point implies the simple connections deduced in the quiescent fluid remain accurate in the nonlinear regime.

V. EFFECT OF BARRIER HOPPING

The analysis in Sec. IV ignores thermally induced barrier hopping, a condition where a rigorous distinction between a liquid and solid can be made and a true yield stress can be defined. In reality, everything flows [58] at "long enough" times due to slow relaxation processes. In this section the

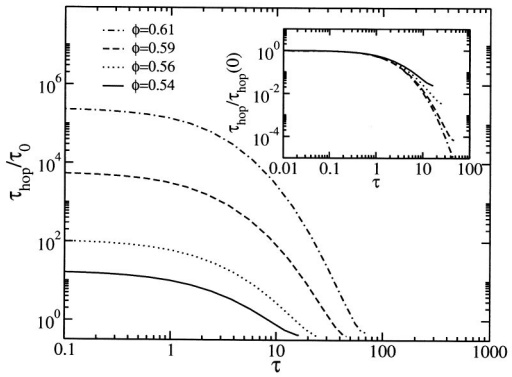

FIG. 9. Dimensionless hopping time as a function of the applied stress for several volume fractions. The inset shows the same results with hopping times normalized by their zero stress values.

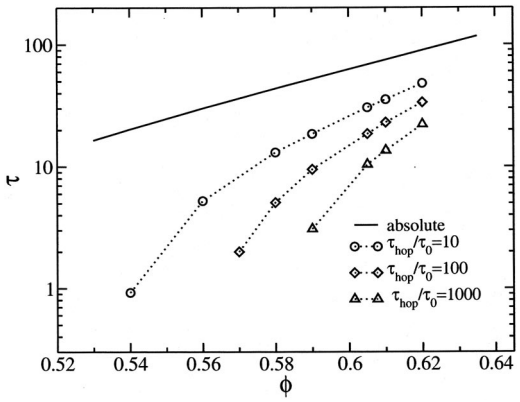

FIG. 10. Dynamic yield stress for three specified time scales. The solid line is the absolute yield stress.

stress, strain, and volume fraction dependences of the barrier hopping time are studied, and a "dynamic yield stress" is determined which separates fluid and solid states in a practical sense. An ultraslow α relaxation process may be the elementary step for aging, creep, and/or sedimentation. Both constant stress and shear rate conditions are examined, which under steady state conditions are equivalent in the absence of rheological instabilities. We note that Barnes and others have vigorously argued that yielding phenomena should be studied using stress, not shear rate, controlled rheology [58], and hence we discuss it first.

A. Stress-controlled rheology

Figure 9 shows the hopping time nondimensionalized by the elementary Brownian time τ_0 as a function of stress for several volume fractions. The elementary Brownian time varies as the particle radius cubed, and for a particle diameter of ~400 nm is typically $\tau_0 \approx 1$ s [4]. The inset presents a normalized plot which shows that the initial stress-induced hopping time reduction occurs in a nearly volume-fraction-independent manner. The curves "splay apart" with increasing stress. A reduction by an order of magnitude requires a dimensionless stress of ~3–5, which corresponds at room temperature to ~1.5–2.5 Pa for a 200 nm colloid.

The dynamic yield stress issue is examined in Fig. 10. The stress required for the hopping time to be a specified value is plotted as a function of volume fraction. Since yielding is now associated with particles going over the barrier, variation of the hopping time scale is meant to mimic the experimental observation time scale on which the glass yields. Results for hopping times of 10, 100, and 1000 times larger than τ_0 are shown. The corresponding absolute yield stress from Fig. 2 is plotted for comparison. There are two interesting trends. A roughly exponential dynamic yield stress dependence is found at high volume fractions with slopes that monotonically increase as the specified time lengthens. At low enough volume fraction a stronger dependence emerges since barriers are low and the specified time is more commensurate with the intrinsic hopping time.

The shear viscosity normalized by its quiescent value [computed using Eqs. (9)–(12)] is presented in Fig. 11(a) as a function of stress. The inset shows the previously determined linear response result [28] (in units of the solvent viscosity), which has been shown to be in good agreement with a compendium of experiments [59] up to relative viscosities of ~3000 at $\phi \approx 0.56$. Over this regime of volume fractions the theoretical results (and also the experimental ones) can be fitted by many different functions including the free volume form, the configurational-entropy-based Adams-Gibbs form, and a critical power law [27,28]. However, the exceptionally wide range of viscosities in Fig. 11(a) allows a more discriminating analysis (although beyond experimental capabilities for colloids). The numerical results are well fit by a strongly supraexponential dependence

$$\frac{\eta(0)}{\eta_0} \cong 8.81 e^{1641\phi^{9.4}}. \tag{25}$$

The rate of change of a relaxation time or viscosity with the system control parameter that induces vitrification is quantified by a "fragility" index m [60]. For athermal colloidal suspensions we define the analog of the thermal fragility as

$$m = \frac{\partial}{\partial \phi} \log_{10} \eta(0) = 6707 \phi^{8.4}, \tag{26}$$

which is a strongly increasing function of volume fraction. It is interesting to contrast the predicted numerical values with thermal liquids. From Eq. (26), $m = 38, 69, 121$ for $\phi = 0.54, 0.58, 0.62$. This range of fragilities largely covers the range observed for thermal glass formers. In particular, $m = 38$ is representative of a relatively "strong" liquid, $m = 69$ a moderately "fragile" liquid, and $m = 121$ an extremely fragile liquid [60]. In deeply supercooled liquids the α relaxation time or shear viscosity at the kinetic glass transition temperature is roughly 8–10 orders of magnitude larger than its value

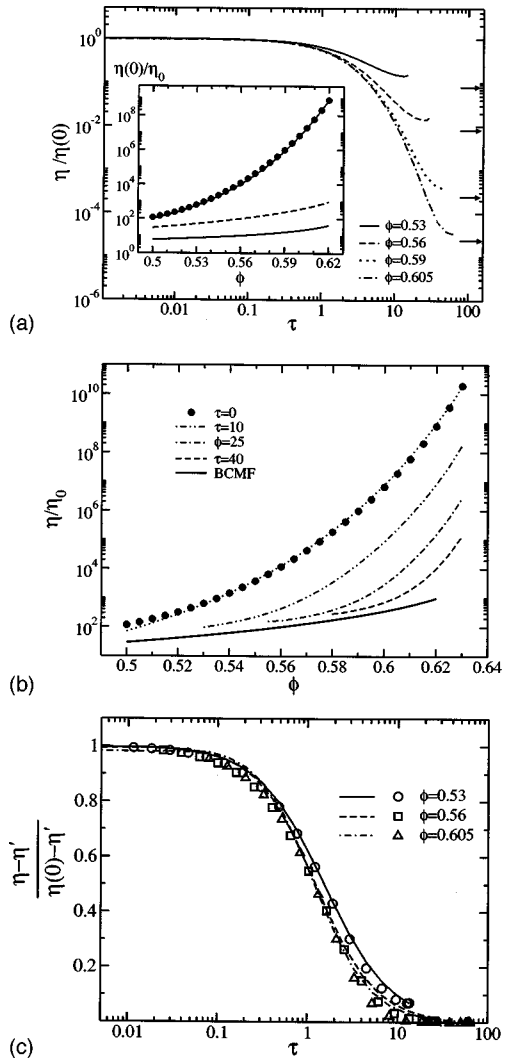

FIG. 11. (a) Shear viscosity normalized by its zero stress value as a function of the applied stress for several volume fractions. Arrows along the right axis indicate the corresponding limiting BCMF viscosity [33]. The inset shows the zero stress viscosity (circles) and the best fit of Eq. (25), the BCMF model viscosity (dashed curve), and the infinite frequency viscosity (solid curve). (b) Relative viscosity as a function of volume fraction for zero and several nonzero stresses (solid circles); a fit using Eq. (28) is also shown. The normal or fluid part of the viscosity given by the BCMF model [33] is also indicated. (c) Reduced differential viscosity as a function of stress for three volume fractions (η' is the BCMF theory of viscosity [33]). Curves are fits to Eq. (30). The corresponding fit parameters are $\tau_{1/2}=1.54,1.23,1.2$ and $m=1.19,1.32,1.42$ for $\phi=0.53,0.56,0.605$.

at a characteristic "crossover temperature" deduced from fitting MCT formulas to experimental data [60]. Using Eq. (25) and our theoretical crossover at $\phi_c=0.432$ where $\eta(0)/\eta_0 \approx 10$ [28], a nine orders of magnitude viscosity ratio is attained at $\phi \cong 0.627$ which corresponds to a very high fragility of ~ 132. From this perspective, athermal colloidal suspensions seem as fragile as molecular liquids or polymer melts.

Various very different mathematical functions also fit the numerical viscosity results. Of particular interest is one motivated by the prior surprising finding that the quiescent suspension entropic barrier is extremely well described (for barriers in excess of the thermal energy) by the formula [27]

$$F_B \cong \frac{0.077}{S_0} - 3.51, \tag{27}$$

where $S(q=0) \equiv S_0 = (1-\phi)^4/(1+2\phi)^2$ is the PY dimensionless compressibility. Since the viscosity directly correlates with stress relaxation and hopping time, one might expect a simple exponential relation between η and the barrier. Figure 11(b) shows this is indeed true since the following expression is very accurate:

$$\frac{\eta(0)}{\eta_0} \cong 0.245 e^{0.092 S_0^{-1}}. \tag{28}$$

The larger prefactor in the exponential [0.092 versus 0.077 in Eq. (27)] arises since the viscosity is qualitatively the product of a relaxation time and a modulus. This interpretation is supported by our finding that the hopping time (not plotted) is extremely well fitted over at least seven orders of magnitude in the range of $\phi=0.52$–0.63 by

$$\frac{\tau_{hop}(0)}{\tau_0} \cong 0.003\,57 e^{0.074 S_0^{-1}}. \tag{29}$$

The accuracy of Eq. (29) reflects the relatively weak dependence on volume fraction of the prefactor in Eq. (8).

The main frame of Fig. 11(a) shows the nonlinear viscosity scaled by its zero stress value as a function of stress. The shapes of the curves are quite similar to the hopping time results in Fig. 9. Rough power law behavior can be identified over rather narrow intervals in the intermediate stress regime, and experiments are sometimes analyzed in such terms. From Fig. 11(a) we find (not plotted) apparent powers laws $\eta/\eta(0) \propto \tau^{-x}$ with exponents of $x \approx 0.7,1.6,3.0,3.9$ with increasing ϕ. The stress-induced viscosity reduction becomes monotonically more abrupt with increasing volume fraction or zero stress viscosity, a trend broadly observed in a wide range of materials [58]. The limiting high stress value of the viscosity is determined by our assumption that stress destroys barriers, but does not affect the "regular" part of the viscosity associated with binary collisions in a mean field cage (BCMF theory [33]). We view this assumption as a crude but reasonable one given the small distortion of local structure seen in experiments and simulations even at relatively high shear rates (before the onset of shear thickening). The regular contribution to the viscosity is volume fraction dependent as reflected by the different levels of reduced viscosity and stress values at which the start of a plateau is seen in Fig. 11(a).

It is interesting to consider the quantitative implications of Fig. 11(a). At $\phi=0.56$ the zero stress reduced viscosity is $\sim 10\,000$, and decreases to ~ 400 at a dimensionless stress of ~ 10 which for a 400 nm colloid corresponds to ~ 0.7 Pa. For stresses below the onset of shear thickening, the theoretical calculations are in good agreement with recent measurements [61] on high volume fraction hard sphere suspensions where the zero stress relative viscosities vary in the range of $\sim 10^3$–10^6.

Figure 11(b) shows the viscosity as a function of volume fraction for different values of constant stress. At nonzero stress the viscosity is computed only for volume fractions above the absolute yield point. The spectacular growth of the viscosity with ϕ is systematically reduced with increasing stress, an effect that could be described as a stress-induced reduction of fragility. The BCMF result is indicated by the solid curve and represents a lower bound or high stress limit.

Figure 11(c) replots the theoretical results in Fig. 11(a) in terms of a reduced differential viscosity $[\eta(\tau)-\eta']/[\eta(0)-\eta']$, a format often adopted by experimentalists [2,4]. Here η' is a "high frequency" limit unaffected by stress, which in our calculation corresponds to the BCMF result [33]. The linear-log format of Fig. 11(c) emphasizes the initial shear thinning regime at intermediate stresses. The calculations are fitted to the popular empirical form [2,4]

$$(\eta-\eta')/(\eta(0)-\eta') \cong [1+(\tau/\tau_{1/2})^{\delta}]^{-1}, \tag{30}$$

where $\eta(\tau_{1/2})/\eta(0) \equiv 0.5$. Experimentally, when (near) hard sphere suspension data are analyzed in this manner the exponent deduced from fits is $\delta \approx 1$–2, and the characteristic dimensionless stress is $\tau_{1/2} \approx 1$–4 and usually a weakly decreasing function of volume fraction for $\phi > 0.5$ [4,45]. The apparent exponent and crossover stress parameters required to fit Eq. (30) to the theoretical results are reported in the figure caption and are consistent with experimental findings [2,4].

Although we do not show more figures, additional calculations indicate that all the basic trends for the viscosity obtained using the Green-Kubo approach are contained in the simple Maxwell model associated with the hopping process

$$\eta_M \equiv G' \tau_{hop}. \tag{31}$$

As can be understood from Eqs. (9)–(12), or Eq. (31), the very strong volume fraction dependence of the Green-Kubo viscosity arises from the relaxation time. For example, as the volume fraction increases from 0.5 to 0.62 the linear response Green-Kubo viscosity increases by seven orders of magnitude while the elastic modulus increases by only one order of magnitude.

Following prior work [28], the stress dependence of the self-diffusion constant can be computed using the Green-Kubo approach [analog of Eqs. (9)–(12)], or even more simply (but still rather accurately [28]) estimated from its hopping analog

$$D_{hop} \equiv L_D^2/6\tau_{hop}. \tag{32}$$

In the linear response regime prior work [28] has shown that the Stokes-Einstein relation is well obeyed, $(D\eta)/(D_0\eta_0) = 2 \pm 1$ for $\phi > 0.5$. Hence, $D \propto \eta^{-1}$ and no significant translation-viscosity "decoupling" [62] is predicted, as expected given the "mean first passage time" analysis of our theory [27,28]. The theory has been recently generalized [63] to include heterogeneity associated with mesoscopic volume fraction fluctuations under quiescent conditions, and the same ideas can be applied to the nonlinear regime.

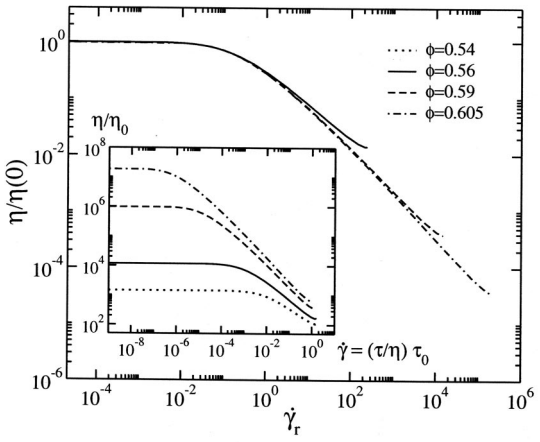

FIG. 12. Viscosity normalized by its zero shear rate value as a function of reduced shear rate defined in Eq. (33). The inset shows the same results for the relative viscosity but with the shear rate in units of the inverse elementary Brownian time τ_0.

B. Shear rate controlled rheology

The inset of Fig. 12 shows results for the viscosity as a function of shear rate in units of the elementary Brownian time $\dot{\gamma}\tau_0$. As expected, with increasing volume fraction the shear thinning process starts at smaller reduced shear rates, and the local power law slope decreases continuously from zero to negative unity. A plateaulike behavior emerges at high shear rates at a viscosity level close to the "normal fluid" contribution described by the BCMF theory [33]. Since $D \propto \eta^{-1} \propto \tau_{hop}^{-1}$, the results in Fig. 12 imply that the diffusion constant will follow a fractional power law dependence on $\dot{\gamma}$ in the intermediate shear rate regime, $D \propto \dot{\gamma}^{\alpha}$, where the apparent exponent α increases from zero to unity followed by a crossover to the normal fluid diffusion constant of the BCMF theory [28,33].

The main panel of Fig. 12 plots the viscosity normalized by its zero shear limit $\eta(0)$ as a function of the shear rate normalized by a characteristic stress relaxation time

$$\dot{\gamma}_r \equiv \dot{\gamma}\tau_{stress}, \quad \tau_{stress} \equiv \eta(0)\beta R^3, \tag{33}$$

where R is the particle radius. This normalization of shear rate is motivated by common experimental analysis. A good collapse of the theoretical results is obtained, as often found experimentally [44–46,52–54] based on the reduced shear rate raised to a power $m \sim 0.8$–1. A characteristic critical

reduced shear rate which quantifies the onset of the shear thinning regime can be defined as when $\eta/\eta(0)=0.5$, from which we predict $\dot{\gamma}_{r,crit}\sim 0.3$. Alternatively, if the critical shear rate is defined from the intersection of the high shear power law with a zero shear horizontal line one obtains $\dot{\gamma}_{r,crit}\sim 0.4$. These values can be compared to high volume fraction experiments [44–46,52–54] which typically find $\dot{\gamma}_{r,crit}\cong 0.2$–$0.4$. Several experimental studies indicate that this value does not exhibit a systematic ϕ dependence [52,54] to within the considerable experimental uncertainties, which is qualitatively consistent with the good universality seen in Fig. 12.

IMCT results for $\eta/\eta(0)$ as a function of reduced shear rate $\dot{\gamma}_r$ based on the full ISHSM and its schematic analog have been recently obtained [16,17]. The calculations are presented in terms of the parameter $\varepsilon\equiv(\phi-\phi_c)/\phi_c$ which quantifies the distance from the quiescent idealized glass transition. For the schematic MCT, and variations of ε corresponding to changes in reduced viscosity (reduced shear rate) by five (four) orders of magnitude, a partial collapse of viscosity curves is found which is considerably less than in Fig. 12; the corresponding $\dot{\gamma}_{r,crit}\approx 0.1$. For the more sophisticated ISHSM version of MCT, a partial collapse of the reduced viscosity versus reduced shear rate data is found for a range of fluid states where the viscosity varies by roughly seven orders of magnitude. The corresponding $\dot{\gamma}_{r,crit}\approx 10$, which is much larger than the results of the schematic MCT model, our theory, and experiment.

The schematic *p*-spin model theory [12,19] predicts an $\eta\propto\dot{\gamma}^{-2/3}$ shear thinning power law at the ideal glass transition, and exponents which approach negative unity deep in the ideal glass state. The former prediction does not appear to agree with IMCT theory. The prediction of IMCT that an infinitesimal shear rate melts the glass is also different than found from the schematic *p*-spin model [12,19]. These differences are not well understood [12].

The corresponding flow curves of stress versus shear rate (in bare Brownian frequency units) for several volume fractions are given in Fig. 13(a). Low shear rate plateaus are not predicted since no true static yield stress exists in the presence of thermal fluctuations and barrier hopping. However, there are rather wide ranges of shear rate where the stress is very slowly varying. The lack of convergence of the high shear regime occurs since the normal fluid (BCMF [33]) contribution is dependent on volume fraction, a feature that has been observed in recent rheological experiments [61].

Motivated by experimental studies and IMCT calculations, an enlargement of the high stress and shear rate regime is given in Fig. 13(b). An apparent power law dependence of the stress on shear rate, $\tau\propto\dot{\gamma}^{\Delta}$, occurs over roughly 2–4 orders of magnitude (increases with ϕ) in shear rate. The effective exponent decreases from $\Delta\approx 0.31$ to $\Delta\approx 0.13$ as volume fraction increases from 0.575 to 0.635. This implies that a power law shear thinning regime exists, $\eta\propto\dot{\gamma}^{-\alpha}$, where $\alpha\approx 0.87$–0.69 as volume fraction decreases from 0.635 to 0.575. The latter corresponds to the *kinetic* glass transition volume fraction, and our theory predicts an *apparent* exponent of $\sim 2/3$. This exponent value is in remarkably good agreement with the schematic *p*-spin MCT-like approach at its *ideal* glass transition point. The reasons for such a connection between the entirely different theories is unclear. For the ISHSM ideal MCT the low shear rate dependence of the stress at the critical volume fraction is $\tau=\tau_{crit}(1+a\dot{\gamma}^{\Delta})$, where $\Delta\approx 0.15$ and $a\sim 0.9$; nearly identical behavior is found for the schematic MCT [16,17]. Curiously our exponent Δ at very high volume fractions is similar to the MCT value. However, the physical significance of this is unclear since there is no true yield stress or ideal glass transition in our theory. Moreover, the power law regime in our theory describes the stress curve in a nonperturbative manner (not as a correction to a nonergodic plateau) and only over a limited range of intermediate shear rates.

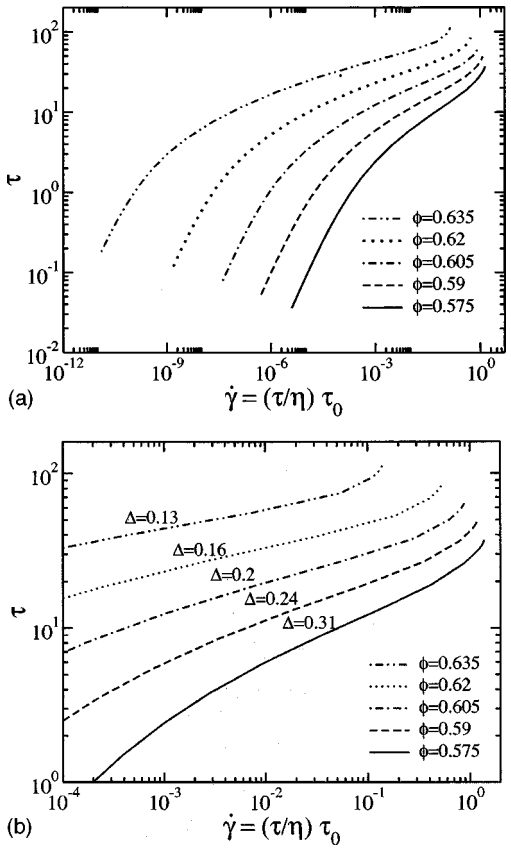

FIG. 13. (a) Stress as a function of shear rate for several volume fractions. (b) Expanded view of (a) in the intermediate shear rate regime often relevant to experiments and simulations. Power law fits $\tau\propto\dot{\gamma}^{\Delta}$ to the middle section of the curves have been made (not shown) and the extracted apparent exponents Δ are indicated.

Recent work has demonstrated that schematic IMCT can provide a good fit of computer simulations of the stress–shear-rate behavior over a few orders of magnitude in shear rate and stress [17]. The agreement is based on modest quantitative adjustments of shear rate and stress to match the simulation results, and more importantly the use of $\varepsilon\equiv(\phi-\phi_c)/\phi_c$ as an adjustable fit parameter. Agreement between simulation and the schematic *p*-spin model approach has also been demonstrated [12,19,26]. However, the caution has been raised [23,26] that activated hopping processes are not taken into account in these theories. The apparent good agreement with simulations may be related to strong limitations of simulations regarding the small range of time scales

and degree of slowing down that are presently feasible to study.

VI. SUMMARY AND CONCLUSIONS

A microscopic theory for the dependence on external strain, stress, and shear rate of the transient localization length, elastic modulus, α relaxation time, shear viscosity, and other dynamic properties of glassy colloidal suspensions has been formulated and quantitatively applied. The relative roles of mechanically driven motion, versus thermally activated barrier hopping and transport, have been studied. Various scaling behaviors are found for the relaxation time and viscosity in both controlled stress and shear rate rheological experiments. Power law and/or exponential dependences of the perturbative and yield stresses on colloid volume fraction, and a nonmonotonic dependence of the absolute yield strain on volume fraction, are predicted. The approach is built on entropic barrier hopping as the elementary physical process. In contrast to ideal MCT and the related schematic *p*-spin approach, an ideal glass or nonergodicity transition plays no role. Our theory does have some aspects in common with MCT and phenomenological trap models, in terms of both underlying ideas and predictions, but it also differs in multiple and fundamental ways. Comparisons of several of our calculations with experiments show encouraging agreement. However, more high volume fraction measurements of both linear and nonlinear viscoelastic properties are required to definitively test the theory.

The theory as presently formulated seems technically and conceptually simpler than MCT and related spin glass approaches. Qualitatively it is a microscopic and predictive "trap model" type approach. However, the simplicity carries limitations, such as the wave-vector-dependent collective dynamic structure factor is not presently amenable to study. The incoherent dynamic structure factor, and other single particle time correlation functions have also not been determined. These single particle quantities can be determined using Brownian dynamics simulation to solve the stochastic nonlinear Langevin equation of motion. All anisotropies associated with the symmetry of the deformation and colloidal structure have been ignored. This appears to be a good first approximation, but distinguishing between different deformations such as shear, uniaxial compressive, hydrostatic, or osmotic requires a full anisotropic generalization. The ideas of the present paper are applicable to these explicitly anisotropic situations, but extra technical effort is required since a multidimensional Kramers activated transport problem must be solved.

Our theory does not predict shear thickening at very high shear rates. This is to be expected given we have ignored many particle hydrodynamic interactions. Recent experiments [64] on large, non-Brownian particle systems suggest shear thickening can also occur in the absence of strong hydrodynamic interactions. This and related experiments have motivated the formulation of nonhydrodynamic ideas within an empirical ideal MCT framework for describing shear thickening [65]. Regardless of the role of hydrodynamics, experiments [49] have clearly shown that shear thickening in Brownian hard sphere suspensions is accompanied by significant flow-induced anisotropies of the structure factor, an aspect not accounted for in our present theory.

The complex issue of a possible violation of the fluctuation-dissipation theorem (FDT) in the nonequilibrium sheared or stressed state has not been addressed in our work, nor by the prior trap model or IMCT-type approaches [9–12,16,17]. Standard Green-Kubo relations are employed in the nonequilibrium steady state. Szamel [66] has analyzed this issue and pointed out that the use of an equilibrium structure approximation for the vertices in MCT is consistent with there being no FDT violation. The former simplification is the analog of our use of equilibrium pair correlations to quantify the "effective free energy" $F(r)$. The fact that a full nonequilibrium stationary steady state probability distribution is not employed does have consequences concerning FDT violation [66], especially for MCT-like theories which have divergent relaxation times in the quiescent state. Since ideal glass transitions do not exist in our theory and ergodicity is always restored via activated barrier hopping, the FDT violation issue seems different and of less concern. More study of this issue is warranted.

Finally, our theory as presently formulated can be immediately applied to treat highly nonlinear dynamical phenomena in other soft glassy complex fluids. These include both external force driven probe motion in dense colloidal suspensions [67] and the nonlinear rheology of depletion gels. Work is in progress on these two problems and will be reported in future publications.

ACKNOWLEDGMENTS

We acknowledge helpful discussions with G. Petekidis, J. A. Lewis and C. F. Zukoski, and correspondence with M. Cates, M. Fuchs, and G. Szamel. This work was supported by the Nanoscale Science and Engineering Initiative of the National Science Foundation under NSF Award No. DMR-0117792.

[1] *Jamming and Rheology: Constrained Dynamics on Microscopic and Macroscopic Scales*, edited by A. J. Liu and S. R. Nagel (Taylor and Francis, London, 2001); H. M. Jaeger, S. R. Nagel, and R. P. Behringer, Rev. Mod. Phys. **68**, 1259 (1996).

[2] R. G. Larson, *The Structure and Rheology of Complex Fluids* (Oxford University Press, New York, 1999).

[3] A. J. Liu and S. R. Nagel, Nature (London), **395**, 21 (1998).

[4] W. B. Russel, D. A. Saville, and W. R. Schowalter, *Colloidal Dispersions* (Cambridge University Press, New York, 1989).

[5] G. M. Gratson, M. Xu, and J. A. Lewis, Nature (London) **428**, 386 (2004).

[6] J. C. Dyre, Phys. Rev. Lett. **58**, 792 (1987); Phys. Rev. B **51**,

12276 (1995).
[7] V. I. Arkhipov and H. Bassler, Phys. Rev. E **52**, 1227 (1995); H. Bassler, Phys. Rev. Lett. **58**, 767 (1987).
[8] C. Monthus and J. P. Bouchaud, J. Phys. A **29**, 3847 (1996); J. P. Bouchaud, L. Cugliandolo, J. Kuchan, and M. Mezard, Physica A **226**, 243 (1996).
[9] R. M. L. Evans, M. E. Cates, and P. Sollich, Eur. Phys. J. B **10**, 705 (1999).
[10] P. Sollich, F. Lequeux, P. Hebraud, and M. E. Cates, Phys. Rev. Lett. **78**, 2020 (1997); P. Sollich, Phys. Rev. E **58**, 738 (1998); S. M. Fielding, P. Sollich, and M. E. Cates, J. Rheol. **44**, 323 (2000).
[11] M. Cates and P. Sollich, J. Rheol. **48**, 193 (2004).
[12] L. Berthier, J. Phys.: Condens. Matter **15**, S933 (2003).
[13] W. Gotze and L. Sjogren, Rep. Prog. Phys. **55**, 241 (1992); W. Gotze, J. Phys.: Condens. Matter **11**, A1 (1999).
[14] W. van Megen and S. Underwood, Phys. Rev. E **49**, 4206 (1994).
[15] W. van Megen, T. C. Mortensen, S. R. Williams, and J. Muller, Phys. Rev. E **58**, 6073 (1998).
[16] M. Fuchs and M. E. Cates, Phys. Rev. Lett. **89**, 248304 (2002); Faraday Discuss. **123**, 267 (2003).
[17] M. Fuchs and M. E. Cates, J. Phys.: Condens. Matter **15**, S401 (2003); M. E. Cates, C. B. Holmes, M. Fuchs, and O. Henrich, e-print cond-mat/0310579
[18] K. Miyazaki and D. R. Reichman, Phys. Rev. E **66**, 050501(R) (2002).
[19] L. Berthier, J. L. Barrat, and J. Kurchan, Phys. Rev. E **61**, 5464 (2000).
[20] L. Berthier and J. L. Barrat, J. Chem. Phys. **116**, 6228 (2002).
[21] R. Yamamoto and A. Onuki, Phys. Rev. E **58**, 3515 (1998).
[22] K. Miyazaki, D. R. Reichman, and R. Yamamoto, Phys. Rev. E **70**, 011501 (2004).
[23] F. Varnik, L. Bocquet, and J. L. Barrat, e-print cond-mat/0309089.
[24] D. L. Malandro and D. J. Lacks, Phys. Rev. Lett. **81**, 5576 (1998); J. Chem. Phys. **110**, 4593 (1999).
[25] D. J. Lacks, Phys. Rev. Lett. **87**, 225502 (2001); Phys. Rev. E **66**, 051202 (2002).
[26] J. L. Barrat, J. Phys.: Condens. Matter **15**, S1 (2003).
[27] K. S. Schweizer and E. J. Saltzman, J. Chem. Phys. **119**, 1181 (2003).
[28] E. J. Saltzman and K. S. Schweizer, J. Chem. Phys. **119**, 1197 (2003).
[29] R. A. Denny, D. R. Reichman, and J. P. Bouchaud, Phys. Rev. Lett. **90**, 025503 (2003); Y. Brumer and D. R. Reichman, Phys. Rev. E **69**, 041202 (2004).
[30] B. Doliwa and A. Heuer, Phys. Rev. E **67**, 030501(R) (2003); **67**, 031506 (2003).
[31] T. R. Kirkpatrick and P. G. Wolynes, Phys. Rev. A **35**, 3072 (1987).
[32] J. P. Hansen and I. R. McDonald, *Theory of Simple Liquids* (Academic, London, 1986).
[33] E. G. D. Cohen, R. Verberg, and I. M. de Schepper, Physica A **251**, 251 (1998).
[34] S. K. Ma, *Modern Theory of Critical Phenomena* (Benjamin, Reading, MA, 1976); N. Goldenfeld, *Lectures on Phase Transitions and the Renormalization Group* (Addison-Wesley, Reading, MA, 1992).
[35] D. Oxtoby in *Liquids, Freezing, and the Glass Transition*, edited by J. P. Hansen, D. Levesque, and J. Zinn-Justin (North-Holland, Amsterdam, 1991).
[36] J. P. Garrahan (private communication); S. Whitelam and J. P. Garrahan, J. Phys. Chem. B **108**, 6611 (2004); F. Ritort and P. Sollich, Adv. Phys. **52**, 219 (2003).
[37] H. A. Kramers, Physica (Amsterdam) **7**, 284 (1940).
[38] C. Kaur and S. P. Das, Phys. Rev. Lett. **86**, 2062 (2000).
[39] K. S. Schweizer (in preparation).
[40] On the L_D scale the inaccuracies of the localized form of $F_0(r)$ in Eq. (7) are more important. The analysis of Ref. [38] suggests that L_D is smaller ($\sim 0.5\sigma$–0.6σ) than the 0.8σ value we employ. However, this is a rather minor ($\sim$ factor of 2) constant numerical prefactor correction to the hopping friction and transport coefficients deduced using Eq. (12), which seems insignificant given the other simplifications employed in our calculations, including the use of PY theory for structural input.
[41] T. G. Mason, H. Gang, and D. A. Weitz, J. Opt. Soc. Am. A **14**, 139 (1997).
[42] Y. L. Chen and K. S. Schweizer, J. Chem. Phys. **120**, 7212 (2004).
[43] G. Petekidis, D. Vlassopoulos, and P. N. Pusey, Faraday Discuss. **123**, 287 (2003); G. Petekidis, A. Moussaid, and P. N. Pusey, Phys. Rev. E **66**, 051402 (2002).
[44] L. B. Chen and C. F. Zukoski, J. Chem. Soc., Faraday Trans. **86**, 2629 (1990).
[45] W. Frith, T. Strivens, and J. Mewis, J. Colloid Interface Sci. **139**, 55 (1990); J. Mewis, W. J. Frith, T. Strivens, and W. B. Russel, AIChE J. **35**, 415 (1989).
[46] P. A. Nommensen, M. H. G. Duits, D. van den Ende, and J. Mellema, Phys. Rev. E **59**, 3147 (1999); P. A. Nommensen, M. H. G. Duits, J. S. Lopulissa, D. van den Ende, and J. Mellema, Prog. Colloid Polym. Sci. **110**, 144 (1998).
[47] T. G. Mason and D. A. Weitz, Phys. Rev. Lett. **75**, 2770 (1995).
[48] H. Watanabe, M. L. Yao, K. Osaki, T. Shokata, H. Niwa, and Y. Morishima, Rheol. Acta **38**, 2 (1999); **37**, 1 (1998).
[49] M. J. Maranzano and N. J. Wagner, J. Chem. Phys. **117**, 10291 (2002).
[50] L. A. Brown, C. F. Zukoski, and L. R. White, AIChE J. **48**, 492 (2002).
[51] M. D. Rintoul and S. Torquato, J. Chem. Phys. **105**, 9258 (1996).
[52] D. Andrew, R. Jones, B. Leary, and D. V. Boger, J. Colloid Interface Sci. **147**, 479 (1991); C. G. de Kruif, E. M. F. van Iersel, A. Vrij, and W. B. Russel, J. Chem. Phys. **83**, 4717 (1985); J. C. van der Werff and C. G. de Kruif, J. Rheol. **33**, 421 (1989).
[53] M. K. Chow and C. F. Zukoski, J. Rheol. **39**, 33 (1995).
[54] L. Marshall and C. F. Zukoski, J. Phys. Chem. **94**, 1164 (1990).
[55] F. Spaepan, Acta Metall. **25**, 407 (1977).
[56] S. Ramakrishnan, Y. L. Chen, K. S. Schweizer, and C. F. Zukoski, Phys. Rev. E **70**, 040401(R) (2004).
[57] R. Buscall, J. McGowan, and A. J. Morton-Jones, J. Rheol. **37**, 621 (1993).
[58] H. A. Barnes, J. Non-Newtonian Fluid Mech. **81**, 133 (1999).
[59] Z. Cheng, J. Zhu, P. M. Chaiken, S. E. Phan, and W. B. Russel, Phys. Rev. E **65**, 041405 (2002).
[60] C. A. Angell, K. L. Ngai, G. B. McKenna, P. F. McMillan, and S. W. Martin, J. Appl. Phys. **88**, 3113 (2000); V. N. Novikov

and A. P. Sokolov, Phys. Rev. E **67**, 031507 (2003).
[61] V. Gopalakrishnan and C. F. Zukoski, J. Rheol. **48**, 1321 (2004).
[62] M. D. Ediger, Annu. Rev. Phys. Chem. **51**, 99 (2000); R. Richert, J. Phys.: Condens. Matter **14**, R703 (2002).
[63] K. S. Schweizer and E. J. Saltzman, J. Phys. Chem. B **108**, 19729 (2004).
[64] E. Bertrand, J. Bibette, and V. Schmitt, Phys. Rev. E **66**, 060401(R) (2002).
[65] C. B. Holmes, M. Fuchs, and M. E. Cates, Europhys. Lett. **63**, 240 (2003).
[66] G. Szamel, Phys. Rev. Lett. **93**, 178301 (2004).
[67] P. Habdas, D. Schaar, A. C. Levitt, and E. R. Weeks, Europhys. Lett. **76**, 477 (2004).